N87-22207

THEORETICAL APPROACH TO OBTAINING DYNAMIC CHARACTERISTICS OF NONCONTACTING SPIRAL-GROOVED SEALS

Takuzo Iwatsubo
Kobe University
Rokko, Nada, Kobe, 657, Japan

Bo-suk Yang
The National Fisheries University of Pusan
599, Daeyon-dong, Nam-ku, Pusan, Korea

Ryuji Ibaraki
Toyota Motor Corporation
1, Toyota-cho, Toyota, 471, Japan

In this paper the dynamic characteristics of spiral-grooved seals are theoretically obtained by using the Navier-Stokes equation. First, with the inertia term of the fluid considered, the flow and pressure in the steady state are obtained for the directions parallel to and perpendicular to the groove. Next, the dynamic character is obtained by analyzing the steady state by analyzing the labyrinth seal.

As a result, the following conclusions were drawn:

(1) As the land width becomes shorter or the helix angle decreases, the cross-coupling stiffness, direct and cross-coupling damping, and add mass coefficients decrease.

(2) As the axial Reynolds number increases, the stiffness and damping coefficients increase. But the add mass coefficient is not influenced by the axial Reynolds number.

(3) The rotational Reynolds number influences greatly the direct and cross-coupling stiffness and direct damping coefficients.

(4) As the journal rotating frequency increases, the leakage flow decreases. Therefore zero net leakage flow is possible at a particular rotating frequency.

INTRODUCTION

High-performance pumps, (i.e., those operating at high rotating speed and high pressure) are used in chemical plants, rocket engines, etc.. These pumps sometimes yield nonsynchronous vibration that is induced by the journal bearings or noncontacting seals. The instability of rotors supported by a journal bearing has been studied very well. However the noncontacting seal, which sometimes induces a nonsynchronous vibration or instability to the pumps, has not been investigated.

The dynamic characteristics of some noncontacting pump seals (the annular plain seal, the tapered seal, and the stepped seal) have been theoretically investigated by Black (refs. 1 and 2), Childs (refs. 3 and 4), and Yang et al. (ref. 5), but there have been no investigations using the theory of fluid dynamics on the parallel-grooved and spiral-grooved seals. Childs studied the parallel-grooved seal by using only a rough approximation. On the other hand, the parallel-grooved labyrinth seal has been investigated by Kostyuk (ref. 6) and Iwatsubo, et al. (ref. 7). For the investigation of the spiral-grooved seal, we studied steady-state characteristics from the viewpoint of leakage. This study was based on investigations of the spiral journal bearing; that is, Whipple (ref. 8) presents a basic idea to analyze the characteristics of the thrust spiral-grooved bearing, Vohr (refs. 9 and 10) and Passera (ref. 11) present an approximate method using creeping flow analysis (which assumes that the groove number is infinitely large), and Zuk (ref. 12) analyzes the static characteristics of the spiral-grooved seal by solving the Navier-Stokes equation with a finite difference method. But all these analyses are for the static characteristics and there are no investigations of the dynamic characteristics.

This paper presents an analytical method to obtain the dynamic characteristics by solving a Navier-Stokes equation with the perturbation method. First the steady-state flow and pressure distribution in the axial direction are obtained by considering the pumping effect due to the spiral groove. Then the dynamic characteristics are obtained at the steady-state condition, and the dynamic force is represented by the matrix form.

SYMBOLS

C_{zo}	mean clearance
D	seal diameter
F	flow induced force
H	thickness of fluid film
I_s	thread number
L	seal length
L_g	groove width
L_l	land width
L_{lg}	L_l/L_g
L_s	number of lands for one thread
NN	number of land and groove sections
P	pressure
ΔP	pressure difference
Q	leakage flow rate

R journal radius

R_a axial Reynolds number

R_e Reynolds number

R_r circumferential Reynolds number

T depth of ditch

t time

u circumferential fluid velocity

w axial fluid velocity

x,y,z coordinates (see fig. 2)

α spiral angle

ε perturbation coefficient

θ divergent flow angle

λ friction coefficient

μ viscous coefficient

ξ loss factor

ξ,η,ζ coordinates (see fig. 2)

ρ density

τ shear stress

Subscripts:

a axial direction

c radial direction

d ditch (mainly used for vortex in ditch)

ex exit

f between clearance flow and cavity flow

g groove

in inlet

j journal

l land

m mean velocity

r circumferential direction

s casing

$(\bar{\cdot})$ time mean

GOVERNING EQUATION AND MODELING OF SPIRAL-GROOVED SEAL

Governing Equation

Figure 1 illustrates the geometry of the spiral-grooved seal. Under the usual assumptions for problems of through flow across annuli with fine clearances, the continuity and momentum equations are represented as follows (ref. 13):

Continuity equation,

$$\frac{\partial H}{\partial t} + \frac{\partial (H u_m)}{\partial x} + \frac{\partial (H w_m)}{\partial z} = 0 \tag{1}$$

where u_m and w_m are mean fluid velocity components in the tangential and axial directions.

Momentum equation in the x-direction,

$$\rho H \left\{ \frac{\partial u_m}{\partial t} + u_m \frac{\partial u_m}{\partial x} + w_m \frac{\partial u_m}{\partial z} \right\} = -H \frac{\partial P}{\partial x} + \tau_{tr} \Big|_0^H \tag{2}$$

Momentum equation in the z-direction,

$$\rho H \left\{ \frac{\partial w_m}{\partial t} + u_m \frac{\partial w_m}{\partial x} + w_m \frac{\partial w_m}{\partial z} \right\} = -H \frac{\partial P}{\partial z} + \tau_{ta} \Big|_0^H \tag{3}$$

Modeling

There are three kinds of spiral-grooved seals, (1) those with the groove on the journal (fig. 1), (2) those with the groove on the casing, and (3) those with grooves on both journal and casing. In this paper the seal with the groove on the journal is analyzed. Figure 2 is an expanded figure of the spiral-grooved seal. Configuration parameters are indicated on this figure; these are spiral angle α, land width L_ℓ, groove width L_g, seal diameter D, and thread number I_s. These parameters are related as follows:

$$\left.\begin{aligned} L &= \pi D \tan\alpha \times L_s \qquad L_g = \frac{\pi D \sin\alpha}{I_s} \times (1 - L_{lg}) \\ L_l &= \frac{\pi D \sin\alpha}{I_s} \times L_{lg} \end{aligned}\right\} \tag{4}$$

where L_s is number of lands for one thread in the axial direction and $L_{\ell g} = L_\ell / Lg$. For the analysis two coordinates are used: one is the η-y-ζ coordinate, which is used for the static analysis and the other is the x-y-z coordinate, which is used for the analysis of dynamic characteristics.

For the analysis the following are assumed:

(1) The fluid is liquid and noncompressible.

(2) Flow in the land in the η-direction is assumed to be a flow between two parallel plates, and flow in the groove is assumed to be a flow in a rectangular cross section and is approximated to the flow in a circular tube.

(3) Flow in the ζ-direction diverges with the angle θ and goes to the next land.

(4) The vortex is formed in the ξ-direction of the groove. But the heat energy is negligibly small.

(5) When the journal deviates a little from the center, the streamline in the groove deviates in the same manner.

DERIVATION OF SHEAR STRESS IN MOMENTUM EQUATION

The shear stress term of equation (3) is derived for the spiral-grooved seal. The friction coefficient of the annular seal is represented by a Reynolds number (ref. 14). But it is very difficult to represent the friction coefficient of the spiral-grooved seal in the same way because the groove is spiral. So the friction coefficient equation derived by Hirs (ref. 15) is used in this analysis. The equation of the friction coefficient between two plates is represented as

$$\lambda = 0.066\, Re^{-0.25} \tag{5}$$

where the velocity used in the Reynolds number is the equivalent mean velocity that includes the pumping action of the spiral-grooved seal. This equivalent mean velocity is used to obtain the shear stress.

Land

The shear stresses of the casing and journal parts in the axial direction (z-direction) $\tau_{\ell sa}, \tau_{\ell ja}$ are represented by the formula for the flow between two parallel plates,

$$\tau_{lsa} = -\tau_{ljа} = \frac{1}{2}\rho\lambda_{la}\omega_{lm}^2 \qquad \lambda_{la} = 0.066\left(\frac{\omega_{lm}H_l}{\nu}\right)^{-0.25} \tag{6}$$

Therefore the shear stress term of equation (3) becomes as

$$\tau_{ta}\Big|_0^H = \tau_{ljа} - \tau_{lsa} = -2\cdot\frac{1}{2}\rho\lambda_{la}\omega_{lm}^2 \tag{7}$$

Groove

In the groove, flow is divided into two regions: the jet flow region and the vortex region. The shear stress of the casing part of the jet region in the axial direction τ_{gsa} is represented by the formula of the flow between two parallel plates,

$$\tau_{gsa} = \frac{1}{2}\rho\lambda_{ga}\omega_{gm}^2 \qquad \lambda_{ga} = 0.066\left(\frac{\omega_{gm}H_g}{\nu}\right)^{-0.25} \tag{8}$$

It is assumed that the energy loss in the groove vortex region is represented by the friction loss between the clearance flow and vortex flow. Assuming that the friction between the vortex and the jet flow λ_f is 0.1 and that the axial velocity component of the vortex w_{dm} is set to one-half of the jet flow w_{gm} (ref. 16), the shear stress of the flow τ_{gfa} becomes

$$\tau_{gfa} = -\frac{1}{2}\rho\lambda_f\left(w_{gm} - w_{dm}\right)^2 = -\frac{1}{2}\rho 0.25\lambda_f\omega_{gm}^2 \tag{9}$$

Therefore the shear stress term in the groove is obtained from equations (8) and (9) as

$$\tau_{ta}\Big|_0^H = \tau_{gfa} - \tau_{gsa} = -\frac{1}{2}\rho 0.25\lambda_f\omega_{gm}^2 - \frac{1}{2}\rho\lambda_{ga}\omega_{gm}^2$$

$$= -\frac{1}{2}\rho\left(\lambda_{ga} + 0.25\lambda_f\right)\omega_{gm}^2 \tag{10}$$

DERIVATION OF STEADY FLOW AND STATIC CHARACTERISTICS

Axial and Circumferential Velocity of Steady Flow

As described before, the η-y-ζ coordinate system is used for the analysis of static characteristics. References 10 and 11 describe investigations of the static characteristics of the spiral-grooved seal. In these investigations, the residual seal pressure is obtained when seal leakage becomes zero because of the pressure induced by spiral pumping action. This residual pressure is a function of the seal configuration, and the seal coefficient can be represented by the nondimensional form. Boon et al. (ref. 17) obtained the

seal coefficient of laminar flow, and Mori, et al. obtained the same by experiment. The seal coefficient $S.C._{laminar}$ for the laminar flow is

$$S.C._{laminar} = \left(\frac{6\mu R\omega}{C_{lo}^2}\right) \Big/ \left(\frac{\Delta P_{laminar}}{L}\right)$$

$$= \frac{\kappa^3(1+\tan^2\alpha)+L_{lg}(1-L_{lg})(\kappa^3-1)^2\tan^2\alpha}{L_{lg}(1-L_{lg})(\kappa^3-1)(\kappa-1)\tan\alpha} \qquad (11)$$

where $\kappa = H_g/H_e$. THe pressure induced by the spiral pumping action $\Delta P_{laminar}$ for the laminar flow is

$$\Delta P_{laminar} = \frac{6\mu R\omega L}{C_{lo}^2} \cdot \frac{L_{lg}(1-L_{lg})(\kappa^3-1)(\kappa-1)\tan\alpha}{\kappa^3(1+\tan^2\alpha)+L_{lg}(1-L_{lg})(\kappa^3-1)^2\tan^2\alpha} \qquad (12)$$

Vohr (ref. 10) compared the seal coefficient for turbulent flow with that for laminar flow by experiment. He obtained the pressure ratio C_t of the seal coefficient of the turbulent and laminar flow as

$$C_t = \frac{\Delta P_{turbulent}}{\Delta P_{laminar}} = 0.0159\ R_r^{0.778} \qquad (13)$$

Then the pressure $\Delta P_{turbulent}$ induced by the spiral pumping action in turbulent flow is

$$\Delta P_{turbulent} = \frac{0.0951\mu R\omega L R_r^{0.778}}{C_{lo}^2}$$

$$\times \frac{L_{lg}(1-L_{lg})(\kappa^3-1)(\kappa-1)\tan\alpha}{\kappa^3(1+\tan^2\alpha)+L_{lg}(1-L_{lg})(\kappa^3-1)^2\tan\alpha} \qquad (14)$$

Since the pressure difference equation (14) acts to resist the pressure difference in the seal ΔP, the pressure difference in the seal becomes smaller than the pressure difference between both seal ends. This pressure difference is called the apparent pressure difference $\Delta P'$; that is,

$$\Delta P' = \Delta P - \Delta P_{turbulent} \qquad (15)$$

This apparent pressure difference acts on the seal and on the fluid flow in the seal. This flow is separated into η- and ζ-directions and the fluid velocities in each direction and in each part are derived in order to calculate the dynamic-flow-induced force in each stage. Then total force is obtained by summing up the lateral force of each stage.

Fluid velocity parallel to groove direction for land. - The relation between the pressure and velocity within the two parallel plates is also considered in the land region;

$$\Delta P' = \frac{1}{2}\rho(1+\xi_{l\eta in})w_{l\eta o}^2 + \frac{1}{2}\rho\lambda_{l\eta}w_{l\eta o}^2\cdot\frac{2L}{C_{lo}\sin\alpha}$$

$$+\frac{1}{2}\rho\left(1-\frac{C_{lo}}{C_{lo}+T^{\infty}}\right)^2 w_{l\eta o}^2 \qquad (16)$$

The first term on the right-hand side of equation (16) represents the inlet pressure loss. The inlet pressure loss of the land is larger than that of the groove because the inlet clearance of the land is smaller than that of the groove and because the fluid flows into the groove. The second term on the right-hand side of equation (16) represents the pressure loss due to wall friction. The third term represents the outlet pressure loss. The value $\lambda_{l\eta}$ is obtained using equation (5), and $\xi_{l\eta in}$ is the inlet pressure loss coefficient, which is 0.5 for the first stage and is represented as follows after the second stage:

$$\left.\begin{aligned}\xi_{l\eta in} &= 1+0.824\delta_2 - (\,1+0.824\delta_1\,)(H_2/H_1\,)^2\\ \delta_1 &= 1.95(\,w_{l0}H_1\,/\,\nu\,)^{-0.43}\\ \delta_2 &= 1.95(\,w_{l0}H_2\,/\,\nu\,)^{-0.43}\end{aligned}\right\} \qquad (17)$$

Therefore if equation (14) is iteratively calculated so that $w_{l\eta 0}$ in function λ coincides with $w_{l\eta 0}$ in equation (16), the flow velocity of the land $w_{l\eta}$ is obtained.

Fluid velocity parallel to the groove direction for groove. - Since the groove is deep enough, the groove is considered to be a rectangular pipe and can be approximated as a circular pipe. The equivalent radius of the rectangular pipe MG (ref. 18) is

$$MG = \frac{L_g(C_{lo}+T)}{2(L_g+C_{lo}+T)} \qquad (18)$$

The friction coefficient of the turbulent circular pipe λ_d (ref. 18) is

$$\lambda_d = 0.791\left(\frac{w_{g\eta o}\cdot 4MG}{\nu}\right)^{-0.25} \tag{19}$$

Therefore the apparent pressure difference $\Delta P'$ is written as follows:

$$\Delta P' = \frac{1}{2}\rho(1+\xi_{g\eta in})w^2_{g\eta o} + \frac{1}{2}\rho\lambda_d w^2_{g\eta o}\frac{L_g}{\sin\alpha}\cdot\frac{1}{MG}$$

$$+ \frac{1}{2}\rho\left(1-\frac{C_{lo}+T}{C_{lo}+T_\infty}\right)^2 w^2_{g\eta o} \tag{20}$$

In this equation the first term on the right-hand side represents the inlet pressure loss of the groove. This inlet pressure loss is smaller than that of the land, because the groove has a larger cross section than the land and because the liquid flows mainly into the groove. The second term represents the pressure loss due to wall friction, and the third term represents the outlet pressure loss of the seal. After $\xi_{g\eta in}$ is obtained by using equation (17), the velocity in the groove in the η-direction $w_{g\eta 0}$ is similarly obtained by iteratively calculating equation (20).

Fluid velocity perpendicular to groove direction. - The flow in the ζ-direction is derived by a method similar to that used to obtain the steady flow of the parallel-grooved seal. Conventional evaluation of the loss of the groove region was not clear. Yamada (ref. 19) obtained the friction coefficient of both the land and the groove by experimental methods. According to his results, as the groove region increases in relation to the land region, the friction coefficient increases as shown in figure 3. This friction coefficient is represented by using the results of reference 19

$$\lambda = 0.26\cdot Re^{-0.24}\cdot 3.31^{1-L_{lg}} \tag{21}$$

From the pressure drop relation the following is obtained:

$$\lambda(L_l+L_g) = \lambda_l L_l + \lambda_g L_g \tag{22}$$

where λ_l is a friction coefficient of flow between two parallel plates. Then the friction coefficient of the groove λ_g is obtained from equations (21) and (22),

$$\lambda_g = 0.26\ Re^{-0.24}\left\{3.31^{1-L_{lg}} + \frac{L_l}{L_g}\left(3.31^{1-L_{lg}} - 1\right)\right\} \tag{23}$$

Therefore the apparent pressure difference in the ζ-direction is obtained by summing each stage of the land and groove, respectively,

$$\Delta P' = \frac{1}{2}\rho(1+\xi_{\zeta in})w_{l\zeta o}^2 + NN\cdot\frac{1}{2}\rho\lambda_{l\zeta}w_{l\zeta o}^2\frac{2L_l}{C_{lo}}$$

$$+ (NN-1)\cdot\frac{1}{2}\cdot\rho\lambda_g w_{l\zeta o}^2\frac{L_g}{2C_{lo}} + \frac{1}{2}\rho\left(1-\frac{C_{lo}}{C_{lo}+T\infty}\right)^2 w_{l\zeta o}^2 \qquad (24)$$

In this equation the first term on the right-hand side represents the inlet pressure loss of the seal, the second and the third terms represent the pressure loss due to wall friction, and the fourth term represents the outlet pressure loss of the seal. The term $\lambda_{l\zeta}$ in this equation is defined in equation (5), $\xi_{\zeta in}$ is defined in equation (17) and NN is the number of the land and groove sections in the ζ-direction. Then the velocity in the ζ-direction $w_{l\zeta 0}$ is obtained by a similar iterative calculation.

Fluid velocity in circumferential and axial directions. - The steady-flow velocity in the x- and z-directions is obtained from the previously calculated steady-flow velocities $w_{l\eta o}$, $w_{g\eta o}$, and $w_{l\zeta o}$ by translating the coordinate system as

$$\begin{pmatrix} u'_{lo} \\ w_{lo} \end{pmatrix} = \begin{pmatrix} \cos\alpha & -\sin\alpha \\ \sin\alpha & \cos\alpha \end{pmatrix}\begin{pmatrix} w_{l\eta o} \\ w_{l\zeta o} \end{pmatrix} \quad \begin{pmatrix} u'_{go} \\ w_{go} \end{pmatrix} = \begin{pmatrix} \cos\alpha & -\sin\alpha \\ \sin\alpha & \cos\alpha \end{pmatrix}\begin{pmatrix} w_{g\eta o} \\ w_{g\zeta o} \end{pmatrix} \qquad (25)$$

where u'_{lo} and u'_{go} are the velocities relative to the journal. Therefore the absolute velocities in the circumferential direction become

$$u_{lo} = V - u'_{lo} \qquad u_{go} = V - u'_{go} \qquad (26)$$

Leakage Flow Rate

Because the leakage flow rates of the land and groove are different, they are considered separately. The leakage flow rate for the land is represented by the relation of the cross-sectional area and velocity,

$$Q_l = I_s \times \frac{L_{lg}}{I_s}\int_{R+T}^{R+T+C_{lo}} w_{lo}\,2\pi r\,dr = \pi C_{lo}\left\{2(R+T)+C_{lo}\right\}L_{lg}w_{lo} \qquad (27)$$

The leakage flow rate for the groove is derived by separating the clearance flow from the cavity flow. The leakage flow rate of the clearance flow in the axial direction is represented as

$$Q_{gc} = I_s \int_0^{L_g/\sin\alpha} w_{go} c_{go} dx$$

$$= I_s \left[\frac{1}{2} L_g (2C_{lo} + L_g \tan\theta) w_{g\eta o} \sin\alpha + \frac{C_{lo} L_g}{\tan\theta} w_{l\zeta o} \right] \quad (28)$$

The leakage flow rate in the cavity is represented by the axial component of cavity flow as

$$Q_{gd} = I_s \times \frac{1 - L_{lg}}{I_s} \int_R^{R+T} w_{go} 2\pi r dr$$

$$= \pi (T + C_{lo})(2R + T + C_{lo})(1 - L_{lg}) w_{go} \quad (29)$$

Therefore the total leakage flow rate for the groove is

$$Q_g = Q_{gc} + Q_{gd} \quad (30)$$

and the total leakage flow rate Q becomes

$$Q = Q_l + Q_g = \pi C_{lo} \{2(R+T) + C_{lo}\} L_{lg} w_{lo}$$

$$+ I_s \left[\frac{1}{2} L_g (2C_{lo} + L_g \tan\theta) w_{g\eta o} \sin\alpha + \frac{C_{lo} L_g}{\tan\theta} w_{l\zeta o} \right]$$

$$+ \pi (T + C_{lo})(2R + T + C_{lo})(1 - L_{lg}) w_{go} \quad (31)$$

Figure 4 shows the leakage flow rate for three types of seal and for L/D = 1.0, a rotating speed of 4000 rpm, and a radial clearance of 0.5 mm. The leakage flow rate for each seal type increased as the pressure difference increased. The leakage flow rate for the parallel-grooved seal was less than that of the land seal. For the spiral-grooved seal, if the spiral angle was small, the leakage flow rate was less than that of the parallel-grooved seal, but if the spiral angle was large, the leakage flow rate was greater than it was for the parallel-grooved seal. For the spiral-grooved seal, if the spiral angle was small and the land width was large, or if the spiral angle was large and the land width was large, the leakage flow rate decreased. For this reason the groove is important for the screw pumping action.

Figure 5 compares the calculated leakage flow rate with experimental results (ref. 20). The groove was on both the journal and casing in this experiment. In the low-speed range the calculated and experimental values were very close, and in the high-speed range the leakage flow rate tended to zero because of gas ingestion phenomenon.

DERIVATION OF PRESSURE DISTRIBUTION

To linearize the equations, a first-order approximation is performed. It is assumed in the linearization that the center of the journal coincides with the center of the casing and that the journal perturbs close to the center. Then the values of fluid film thickness H, pressure P, mean velocity in the z-direction w_m, and mean velocity in the x-direction u_m are written as follows:

$$\left.\begin{aligned} H &= C_o + \varepsilon\psi & P &= P_o + \varepsilon P_1 \\ w_m &= w_o + \varepsilon w_1 & u_m &= u_o + \varepsilon u_1 \end{aligned}\right\} \tag{32}$$

where C_0, P_0, w_0, and u_0 are the steady-state values and ψ, P_1, w_1, and u_1 are the perturbations. The perturbation term in the circumferential direction is neglected because the spiral angle α is usually small and u_1 is sufficiently smaller than w_1.

Pressure Distribution in Steady-State

The steady-state pressure distribution is obtained by substituting equations (7), (10), and (32) into equation (3) and taking the zeroth-order approximation. The pressure gradient of the land in the axial direction is given by

$$\frac{\partial P_{lo}}{\partial z} = -\frac{0.132}{C_{lo}} \cdot \frac{1}{2} \cdot \rho w_{lo}^2 \left(\frac{C_{lo} w_{lo}}{\nu}\right)^{-0.25} \tag{33}$$

The pressure gradient of the groove in the axial direction is given by

$$\frac{\partial P_{go}}{\partial z} = -\frac{1}{2C_{go}} \rho(\lambda_{ga} + 0.25\lambda_f) w_{go}^2 - \rho\left\{u_{go}\frac{\partial w_{go}}{\partial x} + w_{go}\frac{\partial w_{go}}{\partial z}\right\} \tag{34}$$

where C_{go} and w_{go} are functions of z and are represented as

$$C_{go} = C_{lo} + z\tan\theta\cos\alpha \qquad w_{go} = \frac{C_{lo} w_{lo}}{C_{lo} + z\tan\theta\cos\alpha} \tag{35}$$

Therefore equation (31) is written as

$$\frac{\partial P_{go}}{\partial z} = -\frac{1}{2}\frac{\rho(C_{lo}w_{lo})^2 \lambda_{sa}}{2(C_{lo}+z\tan\theta\cos\alpha)^3} - \frac{\rho C_{lo}u_{go}w_{lo}\tan\theta\cos\alpha}{(C_{lo}+z\tan\theta\cos\alpha)^2} \tag{36}$$

where λ_{sa} is the apparent friction coefficient because its dimension is the same as friction; that is,

$$\lambda_{sa} = \lambda_{ga} + 0.25\lambda_f - 2\tan\theta\cos\alpha \tag{37}$$

Dynamic Pressure Distribution

The dynamic pressure distribution is obtained by substituting equations (7), (10), and (32) into the equation of momentum (3) and taking the first-order approximation. For the continuity equation (1) the first-order approximation is also obtained in the same manner. The momentum equation in the axial direction for the land is

$$\frac{\partial P_{l1}}{\partial z} = -\frac{\psi}{C_{lo}}\cdot\frac{\partial P_{go}}{\partial z} + \frac{1}{2C_{lo}^2}\rho 0.033\left(\frac{C_{lo}w_{lo}}{\nu}\right)^{-0.25}\cdot w_{lo}^2\psi$$

$$+\frac{1}{2C_{lo}}\rho 0.033\left(\frac{C_{lo}w_{lo}}{\nu}\right)^{-0.25}\frac{w_{l1}}{w_{lo}}\cdot w_{lo}^2$$

$$-\rho\left\{\frac{\partial w_{l1}}{\partial t} + u_{lo}\frac{\partial w_{l1}}{\partial x} + w_{go}\frac{\partial w_{go}}{\partial z}\right\} \tag{38}$$

The continuity equation is

$$\frac{\partial w_{l1}}{\partial z} = -\frac{1}{C_{lo}}\left(\frac{\partial \psi}{\partial t} + u_{lo}\frac{\partial \psi}{\partial x}\right) \tag{39}$$

Pressure distribution is obtained by solving equations (38) and (39) simultaneously. Equation (39) is the first-order ordinary equation in w_{l1}, and it is solved by setting the boundary condition $w_{l1} = w_{l1}(0)$ at $z = 0$.

$$w_{l1} = w_{l1(0)} - \frac{1}{C_{lo}}\cdot f_l(x,t)\cdot z \tag{40}$$

where

$$f_l(x,t) = \frac{\partial \psi}{\partial t} + u_{lo}\frac{\partial \psi}{\partial x}$$

Substituting equation (40) into equation (38) and setting the boundary condition $P_{\ell 1} = P_{\ell 1}(0)$ at $z = 0$ yield a solution of equation (38). In this boundary condition $P_{\ell 1}(0)$ is the perturbed pressure at the land inlet which is obtained by a first-order approximation of the equation

$$\Delta P = - (1/2)\rho\xi_1 w_m^2 \tag{41}$$

that is,

$$P_{\ell 1(0)} = - \rho\xi_1 w_{\ell o} w_{\ell 1(0)} \tag{42}$$

The term $w_{\ell 1}(0)$ is obtained by neglecting the perturbed pressure at the outlet of the land, (i.e., $z = L_\ell/\cos\alpha$, $P_{\ell 1}(0) = 0$). Then the dynamic pressure of the land $P_{\ell 1}$ is obtained as

$$P_{\ell 1} = \frac{1}{2C_{\ell o}^2}\rho w_{\ell o} 0.165\left(\frac{C_{\ell o} w_{\ell o}}{\nu}\right)^{-0.25} \psi \cdot SPL1 - \frac{1}{2C_{\ell o}^2}\rho w_{\ell o} 0.033\left(\frac{C_{\ell o} w_{\ell o}}{\nu}\right)^{-0.25}$$

$$\times \frac{1}{2w_{\ell o}} \cdot f_\ell(x,t) \cdot SPL2 + \frac{1}{C_{\ell o}}\rho w_{\ell o} \cdot f_\ell(x,t) \cdot SPL1$$

$$+ \frac{1}{2C_{\ell o}}\rho\left(\frac{\partial}{\partial t} + u_{\ell o}\frac{\partial}{\partial x}\right) f_\ell(x,t)\ SPL2 \tag{43}$$

where SPL1 and SPL2 are as written in appendix A.

The momentum equation in the axial direction for the groove is

$$\frac{\partial P_{g1}}{\partial z} = - \frac{\psi}{C_{go}} \cdot \frac{\partial P_{go}}{\partial z} - \frac{\rho}{C_{go}}(\lambda_{ga} + 0.25\lambda_f) w_{go} w_{g1}$$

$$- \rho\left\{\frac{\partial w_{g1}}{\partial t} + w_{go}\frac{\partial w_{g1}}{\partial z} \times \tan\alpha + u_{go}\frac{\partial w_{g1}}{\partial x} + w_{g1}\frac{\partial w_{go}}{\partial z}\right.$$

$$\left. + \frac{\psi w_{go}}{C_{go}} \cdot \frac{\partial w_{go}}{\partial z} + \frac{\psi u_{go}}{C_{go}} \cdot \frac{\partial w_{go}}{\partial z} \times \tan\alpha \right\} \tag{44}$$

The continuity equation is

$$\frac{\partial \psi}{\partial t} + u_{go}\frac{\partial \psi}{\partial x} + \psi\frac{\partial w_{go}}{z} + w_{g1}\frac{\partial C_{go}}{\partial z} + C_{go}\frac{\partial w_{g1}}{\partial z} = 0 \tag{45}$$

Substituting equation (36) into equation (45) and setting the boundary condition $w_{g1} = w_{g1(0)}$ at $z = 0$ yield the solution of equation (45):

$$w_{g1} = w_{g1(0)} \cdot \frac{C_{lo}}{C_{lo}+z\tan\theta\cos\alpha} - \frac{z}{C_{lo}+z\tan\theta\cos\alpha} \cdot f_g(x,t) + \frac{\psi w_{lo}\, z\tan\theta\cos\alpha}{(C_{lo}+z\tan\theta\cos\alpha)^2} \qquad (46)$$

where

$$f_g(x,t) = \frac{\partial\psi}{\partial t} + u_{go}\frac{\partial\psi}{\partial x}$$

Substituting equations (36) and (46) into equation (44) and setting the boundary condition $P_{g1} = P_{g1(0)}$ at $z = 0$ yield the solution of equation (44), where $P_{g1(0)}$ is the pressure loss at the inlet of the groove: that is, the outlet loss of the land. The outlet loss of the land is represented by

$$\Delta P_{lex} = \frac{1}{2}\rho\xi_2 w_{lo}^2 \qquad (47)$$

where ξ_2 is the outlet loss coefficient

$$\xi_2 = \left(1 - \frac{C_{lo}}{C_{lo}+L_g\tan\theta}\right)^2 \qquad (48)$$

The first approximation of equation (47) is represented as

$$P_{g1}(z_n) = -\rho\xi_2 w_{lo} w_{g1}(z_n) \qquad (49)$$

The term $w_{g1}(0)$ is obtained by neglecting the perturbed pressure at the groove outlet; that is, $z = L_g/\cos\alpha$, $P_{g1} = 0$. Then the dynamic pressure of the groove is obtained as

$$P_{g1} = -\frac{\rho C_{lo}^2 w_{lo}^2 \lambda_{sa}}{6\tan\theta\cos\alpha}\cdot\psi\cdot SPG3 - \frac{\rho C_{lo} w_{lo}}{\tan\theta\cos\alpha} f_g(x,t)\cdot SPG1$$

$$-\frac{\rho C_{lo} w_{lo}^2 \lambda_{sa}}{\tan\theta\cos\alpha}\psi\cdot SPG6 + \frac{\rho C_{lo} w_{lo} \lambda_{sa}}{(\tan\theta\cos\alpha)^2} f_g(x,t)\cdot SPG7$$

$$-\frac{\rho\omega_{lo}}{(\tan\theta\cos\alpha)} f_g(x,t)\cdot SPG8$$

$$+\frac{\rho}{(\tan\theta\cos\alpha)^2}\left(\frac{\partial}{\partial t}+u_{go}\frac{\partial}{\partial x}\right)f_g(x,t)\cdot SPG9 \qquad (50)$$

where SPG1 to SPG9 are represented in appendix B.

DYNAMIC FORCE

The small displacements in the X- and Y-directions at the center, ΔX and ΔY respectively, are as follows:

$$\varepsilon\psi = -\Delta X\cos\phi - \Delta Y\sin\phi \qquad (51)$$

The flow-induced forces in the X- and Y-directions at the beginning of a land ϕ_n, at the beginning of a groove $\phi_{n+1/2}$, and at the beginning of the next land section ϕ_{n+1} are represented by equations (52) and (53).

$$F_X = -\sum_{n=1}^{I_s}\left[\int_{\phi_n}^{\phi_{n+1/2}}\left\{\int_{L_l/\cos\alpha-R(\phi-\phi_n)\tan\alpha}^{L_l/\cos\alpha}\varepsilon P_{l1in}\,dz\right.\right.$$

$$+L_s\cdot I_s\int_0^{L_g/\cos\alpha}\varepsilon P_{g1}\,dz+(L_s\cdot I_s-1)\int_0^{L_l/\cos\alpha}\varepsilon P_{l1}\,dz$$

$$\left.+\int_0^{L_l/\cos\alpha-R(\phi-\phi_n)\tan\alpha}\varepsilon P_{l1ex}\,dz\right\}\times R\cos\phi\,d\phi$$

$$+\int_{\phi_{n+1/2}}^{\phi_{n+1}}\left\{\int_{L_g/\cos\alpha-R(\phi-\phi_{n+1/2})\tan\alpha}^{L_g/\cos\alpha}\varepsilon P_{g1in}\,dz\right.$$

$$+L_s\cdot I_s\int_0^{L_l/\cos\alpha}\varepsilon P_{l1}\,dz+(L_s\cdot I_s-1)\int_0^{L_g/\cos\alpha}\varepsilon P_{g1}\,dz$$

$$\left.\left.+\int_0^{L_g/\cos\alpha-R(\phi-\phi_{n+1/2})\tan\alpha}\varepsilon P_{g1ex}\,dz\right\}\times R\cos\phi\,d\phi\right] \qquad (52)$$

$$F_Y = -\sum_{n=1}^{I_s}\Bigg[\int_{\phi_n}^{\phi_{n+1/2}}\Bigg\{\int_{L_l/\cos\alpha-R(\phi-\phi_n)\tan\alpha}^{L_l/\cos\alpha}\varepsilon P_{l1in}\,dz + L_s\cdot I_s\int_0^{L_g/\cos\alpha}\varepsilon P_{g1}\,dz + (L_s\cdot I_s-1)\int_0^{L_l/\cos\alpha}\varepsilon P_{l1}\,dz + \int_0^{L_l/\cos\alpha-R(\phi-\phi_n)\tan\alpha}\varepsilon P_{l1ex}\,dz\Bigg\}\times R\sin\phi\,d\phi + \int_{\phi_{n+1/2}}^{\phi_{n+1}}\Bigg\{\int_{L_g/\cos\alpha-R(\phi-\phi_{n+1/2})\tan\alpha}^{L_g/\cos\alpha}\varepsilon P_{g1in}\,dz + L_s\cdot I_s\int_0^{L_l/\cos\alpha}\varepsilon P_{l1}\,dz + (L_s\cdot I_s-1)\int_0^{L_g/\cos\alpha}\varepsilon P_{g1}\,dz + \int_0^{L_g/\cos\alpha-R(\phi-\phi_{n+1/2})\tan\alpha}\varepsilon P_{g1ex}\,dz\Bigg\}\times R\sin\phi\,d\phi\Bigg] \tag{53}$$

This force may be represented in the following matrix form:

$$-\begin{bmatrix}F_X\\F_Y\end{bmatrix} = \begin{bmatrix}K_{XX} & K_{XY}\\K_{YX} & K_{YY}\end{bmatrix}\begin{bmatrix}X\\Y\end{bmatrix} + \begin{bmatrix}C_{XX} & C_{XY}\\C_{YX} & C_{YY}\end{bmatrix}\begin{bmatrix}\dot{X}\\\dot{Y}\end{bmatrix} + \begin{bmatrix}M_{XX} & M_{XY}\\M_{YX} & M_{YY}\end{bmatrix}\begin{bmatrix}\ddot{X}\\\ddot{Y}\end{bmatrix} \tag{54}$$

The following coefficients are obtained from equations (52) to (54). The dynamic coefficients are different for the land and the groove.

$$K_{XXl} = \frac{\rho\pi R}{2C_{lo}}\left[-\frac{w_{lo}^2}{C_{lo}}\,0.165\left(\frac{C_{lo}w_{lo}}{\nu}\right)^{-0.25}\cdot ISPL1 + \left(\frac{u_{lo}}{R}\right)^2 ISPL2\right] = K_{YYl}$$

$$K_{YXl} = \frac{\rho\pi u_{lo}w_{lo}}{C_{lo}}\left[-\frac{1}{4C_{lo}}\,0.033\left(\frac{C_{lo}w_{lo}}{\nu}\right)^{-0.25}\cdot ISPL2 + ISPL1\right] = -K_{XYl}$$

$$C_{XXl} = \frac{\rho\pi R w_{lo}}{C_{lo}}\left[+\frac{1}{4C_{lo}}\,0.033\left(\frac{C_{lo}w_{lo}}{\nu}\right)^{-0.25}\cdot ISPL2 - ISPL1\right] = C_{YYl} \qquad (55)$$

$$C_{YXl} = +\frac{\rho\pi u_{lo}}{C_{lo}}\cdot ISPL2 = -C_{XYl} \qquad M_{XXl} = -\frac{\rho\pi R}{2C_{lo}}\cdot ISPL2 = M_{YYl}$$

$$M_{YXl} = M_{XYl} = 0$$

$$K_{XXg} = \frac{\rho\pi R}{\tan\theta\cos\alpha}\left[\frac{C_{lo}^2 w_{lo}^2 \lambda_{sa}}{6}\cdot ISPG3 + C_{lo}w_{lo}^2\lambda_{sa}\cdot ISPG6 + \frac{1}{\tan\theta\cos\alpha}\left(\frac{u_{go}}{R}\right)^2\cdot ISPG9\right] = K_{YYg}$$

$$K_{YXg} = -\frac{\rho\pi C_{lo}w_{lo}u_{go}}{\tan\theta\cos\alpha}\left[ISPG1 - \frac{\lambda_{sa}}{\tan\theta\cos\alpha}\cdot ISPG7 + \frac{1}{C_{lo}}\cdot ISPG8\right] = -K_{XYg} \qquad (56)$$

$$C_{XXg} = \frac{\rho\pi R C_{lo}w_{lo}}{\tan\theta\cos\alpha}\left[ISPG1 - \frac{\lambda_{sa}}{\tan\theta\cos\alpha}\,ISPG7 + \frac{1}{C_{lo}}\,ISPG8\right] = C_{YYg}$$

$$C_{YXg} = \frac{2\rho\pi u_{go}}{(\tan\theta\cos\alpha)^2}\cdot ISPG9 = -C_{XYg}$$

$$M_{XXg} = -\frac{\rho\pi R}{(\tan\theta\cos\alpha)^2}\,ISPG9 = M_{YYg} \qquad M_{YXg} = M_{XYg} = 0$$

where ISPL2 to ISPG9 are represented in appendix C.

The coefficient matrix represents the summation of the coefficients of the land and the groove.

NUMERICAL EXAMPLE

Data for the seal model are shown in table I. Figure 6 shows the relation between the axial Reynolds number (pressure difference between the inlet and outlet of the seal) and the spiral angle α, where L/D = 1.0, rotating speed is 3000 rpm, and pressure difference between inlet and outlet is 0.49 to 4.9 MPa. As Reynolds number in the axial direction increases, K_{xx}, K_{yx}, C_{xx}, and C_{yx} increase, but M_{xx} is almost constant. For the 3-thread 2.6° spiral-angle spiral-grooved seal and the 20-thread 17.66° spiral-angle spiral-grooved seal, the dynamic coefficient decreases as the spiral angle decreases.

Figure 7 shows the effects of the Reynolds number in the axial direction and the ratio of the land width to the groove width. It is known that as the land width increases, the coefficients K_{xx}, K_{yx}, C_{xx}, C_{yx}, and M_{xx} increase and that, if the land is narrow, the spring coefficient K_{xx} becomes negative.

Figure 8 shows the effect of the circumferential Reynolds number for two kinds of spiral-grooved and parallel-grooved seals, where L/D = 1.0, the pressure difference between the inlet and outlet is 0.49 to 4.9 MPa, and rotating speed is 2000 to 8000 rpm. Coefficient K_{xx} of the spiral-grooved seal shows a negative value for a low circumferential Reynolds number, but that of the parallel-grooved seal does not show a negative value until a high circumferential Reynolds number is obtained. The reason is that the pressure difference between the inlet and outlet of the spiral groove seal affects the circumferential velocity; that is, the pressure difference and the high rotating speed induce the pumping action, and the apparent pressure difference becomes small. The characteristics of the coefficients K_{xy} and C_{xx} can be illustrated in the same way. The values of the coefficients K_{yx}, C_{xx}, C_{yx}, and M_{xx} for the spiral-grooved seal are larger than those for the parallel-grooved seal.

CONCLUSIONS

From this study of the dynamic characteristics of noncontacting spiral-grooved seals, the following conclusions are drawn:

1. Except for K_{xx}, coefficients become small as the spiral angle and the land width decrease.

2. As the axial Reynolds number increases, coefficients K_{xx}, K_{yx}, C_{xx}, and C_{yx} become large but M_{xx} remains constant.

3. As the circumferential Reynolds number increases, K_{xx} decreases, K_{yx} and C_{xx} increase once and then decrease, C_{yx} increases, and M_{xx} is almost constant.

4. The coefficient K_{xx} becomes negative when the circumferential Reynolds number is large and the axial Reynolds number is small.

5. Leakage flow decreases as the rotating speed becomes large. If the spiral angle is small, leakage flow decreases as the groove width becomes large, and if the spiral angle is large, the leakage flow decreases as the groove width becomes small.

6. Comparing the coefficients of the spiral-grooved seal with those of the parallel-grooved seal, yields the following conclusions:

a. K_{xx} of the spiral-grooved seal is smaller than that of the parallel-grooved seal.

b. K_{yx} and C_{xx} of the spiral-grooved seal are smaller (larger) than they are for the parallel-grooved seal for low (high) circumferential Reynolds numbers, respectively.

c. C_{yx} and M_{xx} of the spiral-grooved seal are larger than they are for the parallel-grooved seal.

d. Leakage flow of the spiral-grooved seal is larger (smaller) than that of the parallel-grooved seal for low (high) rotating speeds, respectively.

APPENDIX A

$$q_l = \rho w_{lo} \xi_1 - \frac{1}{2C_{lo}} \rho w_{lo} 0.033 \left(\frac{C_{lo} w_{lo}}{\nu} \right)^{-0.25} \cdot \frac{L_l}{\cos\alpha}$$

$$q_{l1} = \rho w_{lo} \xi_1$$

$$q_{l2} = \frac{1}{2C_{lo}} \rho w_{lo} 0.033 \left(\frac{C_{lo} w_{lo}}{\nu} \right)^{-0.25}$$

$$SPL1 = z - \frac{1}{q_l} \{ q_{l1} - q_{l2} \cdot z \} \frac{L_l}{\cos\alpha}$$

$$SPL2 = z^2 - \frac{1}{q_l} \{ q_{l1} - q_{l2} \cdot z \} \left(\frac{L_l}{\cos\alpha} \right)^2$$

APPENDIX B

$$C_{g1} = C_{lo} + L_g \tan\theta$$

$$q_{g1} = \rho w_{lo} (1 - C_{lo}/C_{g1})^2$$

$$q_{g2} = - \frac{\rho C_{lo}^2 w_{lo} \lambda_{sa}}{2 \tan\theta \cos\alpha}$$

$$m = \frac{1}{q_g} \left\{ q_{g1} + q_{g2} \left(\frac{1}{C_{go}^2} - \frac{1}{C_{lo}^2} \right) \right\}$$

$$SPG1 = 1/C_{go} - 1/C_{lo} - m \cdot K1$$

$$SPG2 = 1/C_{go}^2 - 1/C_{lo}^2 - m \cdot K2$$

$$SPG3 = 1/C_{go}^3 - 1/C_{lo}^3 - m \cdot K3$$

$$SPG4 = \ln(C_{go}/C_{lo}) - m \cdot K4$$

$$SPG5 = C_{go} - C_{lo} - m \cdot K5$$

$$SPG6 = - \frac{1}{2} SPG2 + \frac{C_{lo}}{3} SPG3$$

$$SPG7 = -SPG1 + \frac{C_{lo}}{2} SPG2$$

$$SPG8 = C_{lo} \cdot SPG1 + SPG4$$

$$SPG9 = -C_{lo} \cdot SPG4 + SPG5$$

$$K1 = 1/C_{g1} - 1/C_{lo} \qquad K2 = 1/C_{g1}^2 - 1/C_{lo}^2$$

$$K3 = 1/C_{g1}^3 - 1/C_{lo}^3 \qquad K4 = \ln(C_{g1}/C_{lo})$$

$$K5 = C_{g1} - C_{lo} \qquad K6 = C_{g1}^2 - C_{lo}^2$$

$$K7 = q_{g1}/q_g \qquad K8 = q_{g2}/q_g$$

APPENDIX C

$$ISPL1 = \frac{1}{2}\left(\frac{L_l}{\cos\alpha}\right)^2 + \frac{q_{l2}}{2q_l}\left(\frac{L_l}{\cos\alpha}\right)^3 - \frac{q_{l1}}{q_l}\left(\frac{L_l}{\cos\alpha}\right)^2$$

$$ISPL2 = \frac{1}{3}\left(\frac{L_l}{\cos\alpha}\right)^3 + \frac{q_{l2}}{2q_l}\left(\frac{L_l}{\cos\alpha}\right)^4 - \frac{q_{l1}}{q_l}\left(\frac{L_l}{\cos\alpha}\right)^3$$

$$ISPG1 = \frac{K4}{\tan\theta\cos\alpha} + \frac{K8 \cdot K1^2}{\tan\theta\cos\alpha} - \left(\frac{1}{C_{lo}} + K7 \cdot K1 - \frac{K8 \cdot K1}{C_{lo}^2}\right)\frac{L_g}{\cos\alpha}$$

$$ISPG2 = -\frac{K1}{\tan\theta\cos\alpha} + \frac{K8 \cdot K1 \cdot K2}{\tan\theta\cos\alpha} - \left(\frac{1}{C_{lo}^2} + K7 \cdot K2 - \frac{K8 \cdot K2}{C_{lo}^2}\right)\frac{L_g}{\cos\alpha}$$

$$ISPG3 = -\frac{K2}{2\tan\theta\cos\alpha} - \frac{K8 \cdot K1 \cdot K3}{\tan\theta\cos\alpha} - \left(\frac{1}{C_{lo}^3} + K7 \cdot K3 + \frac{K8 \cdot K3}{C_{lo}^2}\right)\frac{L_g}{\cos\alpha}$$

$$ISPG4 = \frac{1}{\tan\theta\cos\alpha}\left\{\ln(C_{g1}/C_{lo})-K5\right\}-\frac{K8\cdot K1\cdot K4}{\tan\theta\cos\alpha} - \left(\ln C_{lo}+K7\cdot K4+\frac{K8\cdot K4}{C_{lo}^2}\right)\frac{L_g}{\cos\alpha}$$

$$ISPG5 = \frac{K6}{2\tan\theta\cos\alpha}-\frac{K8\cdot K1\cdot K5}{\tan\theta\cos\alpha}-\left(C_{lo}+K7\cdot K5+\frac{K8\ K5}{C_{lo}^2}\right)\frac{L_g}{\cos\alpha}$$

$$ISPG6 = -\frac{1}{2}\,ISPG2 + \frac{C_{lo}}{3}\,ISPG3$$

$$ISPG7 = -ISPG1 + \frac{C_{lo}}{2}\,ISPG2$$

$$ISPG8 = C_{lo}\,ISPG1 + ISPG4$$

$$ISPG9 = -C_{lo}\,ISPG4 + ISPG5$$

REFERENCES

1. Black, H.F.: J. Mech. Sci., 12-4, 1970, 301.
2. Black, H.F.: Proc. 9th Int'l. Conf. Fluid Sealing, 1981, D4-141.
3. Childs, D.W.: Trans. ASME, Ser. F, 105-3, 1983, 429.
4. Childs, D.W.: Trans. ASME, Ser. F, 105-3, 1983, 437.
5. Yang, B., et al.: Trans. JSME, Ser. C, 49-45, 1983, 1636.
6. Kostyuk, A.G.: Teploenergetica, 1975, Vol. 22, No. 3, 41.
7. Iwatsubo, T., et al.: Flow Induced Force of Labyrinth Seal. Rotordynamic Instability Problems in High-Performance Turbomachinery. NASA CP-2250, 1982, pp. 205-222.
8. Whipple, R.T.P.: AERE Report T/R 622, 1958.
9. Vohr, J.H.: Trans. ASME, Ser. D, 87-3, 1965, 568.
10. Vohr, J.H.: Proc. 4th Int'l. Conf. Fluid Sealing, 1969, 311.
11. Passera, W.: Proc. 5th Int'l. Conf. Fluid Sealing, 1971, B6-89.
12. Zuk, J.: NASA TN D-3635, 1966.

13. Iwatsubo, T., et al.: Rotordynamic Instability Problems in High-Performance Turbomachinery Workshop, 1986.

14. Yamada, Y.: Trans. JSME, 26-180, 1961, 1267.

15. Hirs, G.G.: Trans. ASME, Ser. F, 96-1, 1974, 118.

16. Hauck, L.: IFTOMM paper, 1982, 361.

17. Boon, E.F.: Chemie. Ing. Tech., 31-3, 1959, 202.

18. Edited by JSME, Fluid Resistance in Pipe and Duct, 1980, 48.

19. Yamada, Y.: Trans. JSME, 25-171, 1960, 1514.

20. Kawakami, T., Kanki, H.: Private Information.

TABLE I. - DATA FOR NUMERICAL CALCULATION

Working fluid	water
Fluid temperature, K	293.15
Density, ρ, Kg/m^3	9.982×10^2
Viscosity, μ, mPa s	1.009
Kinematic viscosity, ν, m^2/s	1.006×10^{-6}
Journal radius, R, mm	100.0
Seal radial clearance, C_{ro}, mm	0.4
Seal length, L, mm	200.0
Groove depth, T, mm	1.18
Helix angle, α, deg	1.30 to 17.66
Journal rotating frequency, N, rpm	2000 to 8000
Pressure difference, ΔP, MPa	0.49 to 4.9

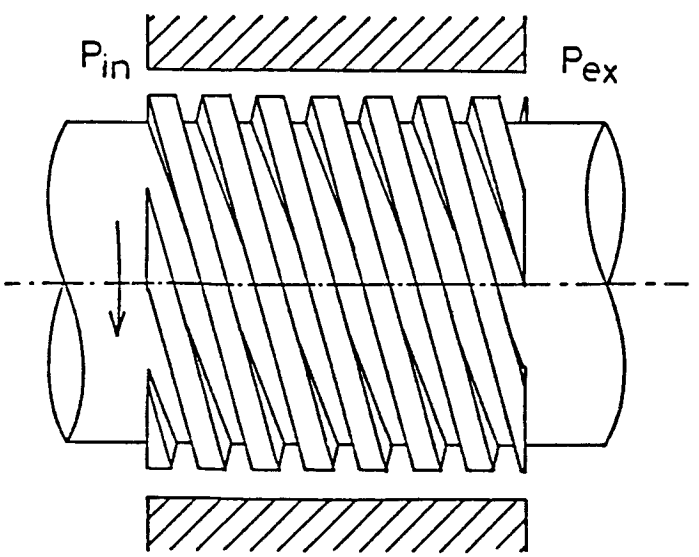

Figure 1. - Spiral-grooved seal.

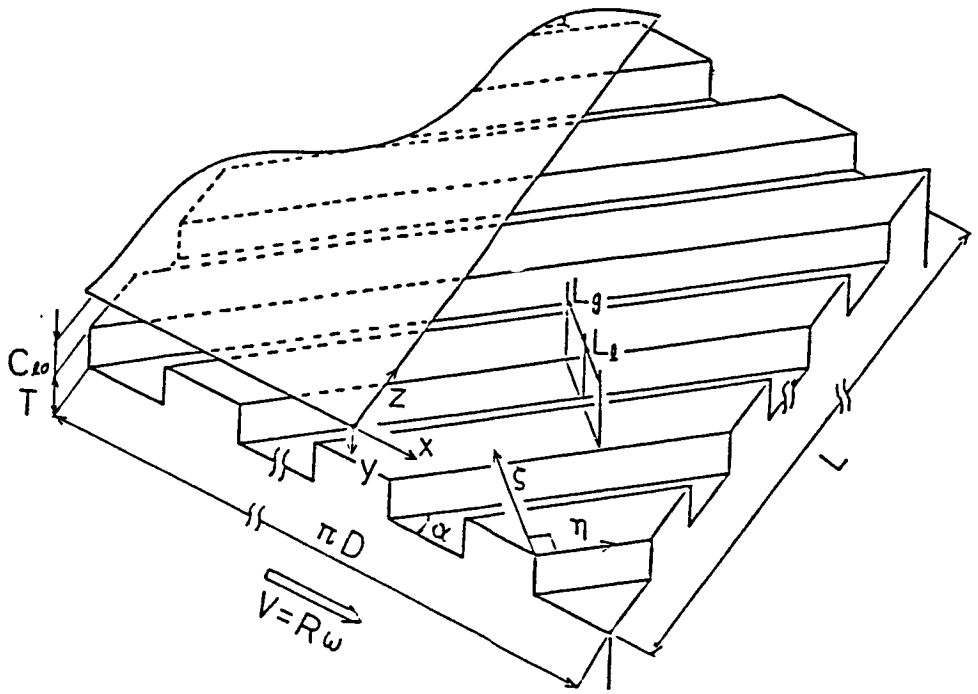

Figure 2. - Illustration of spiral-grooved seal.

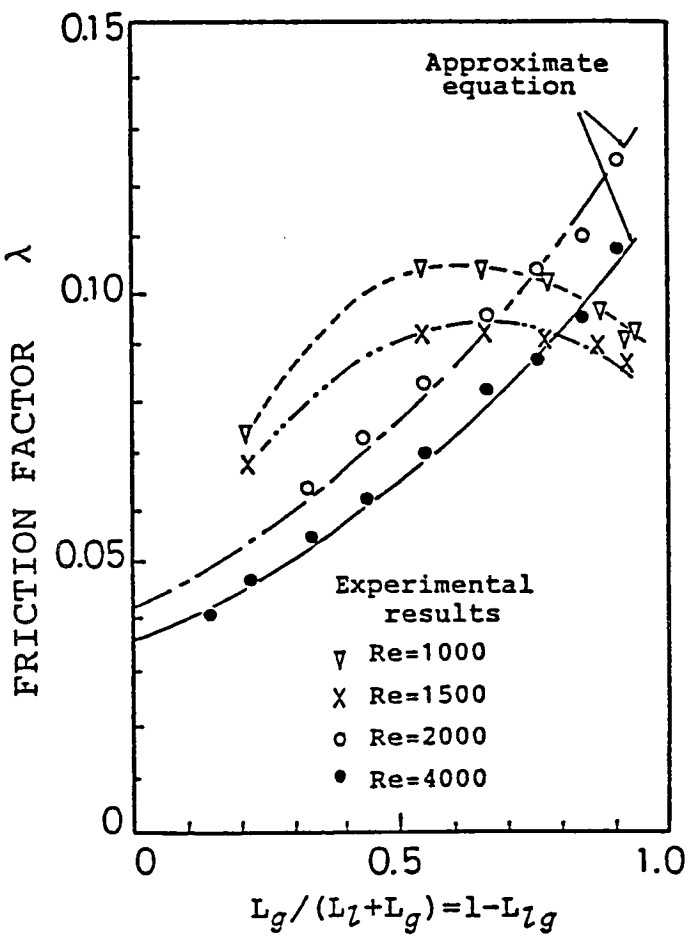

Figure 3. - Friction coefficients.

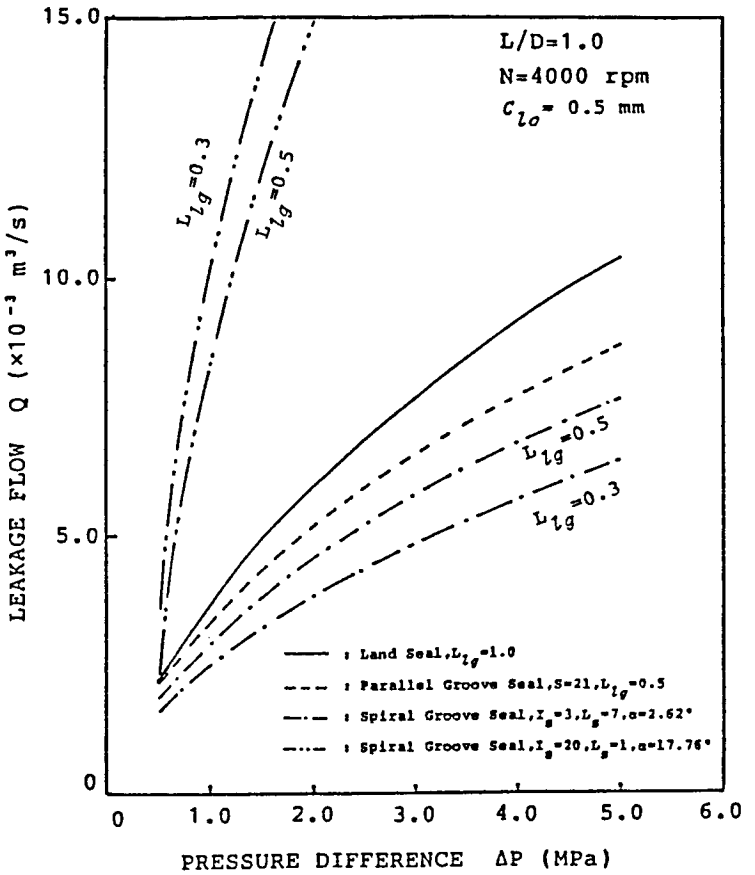

Figure 4. - Leakage flow versus pressure difference.

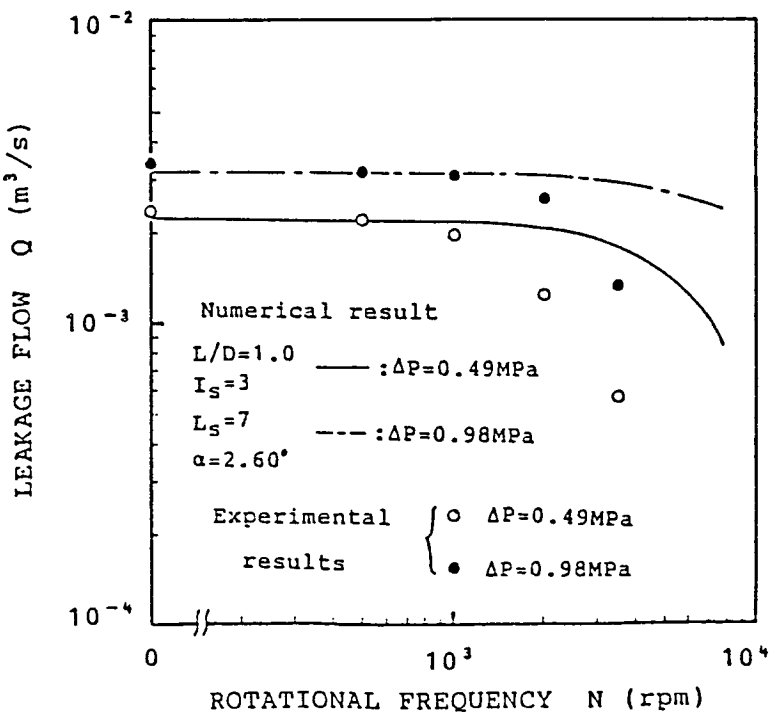

Figure 5. - Leakage flow versus rotating speed.

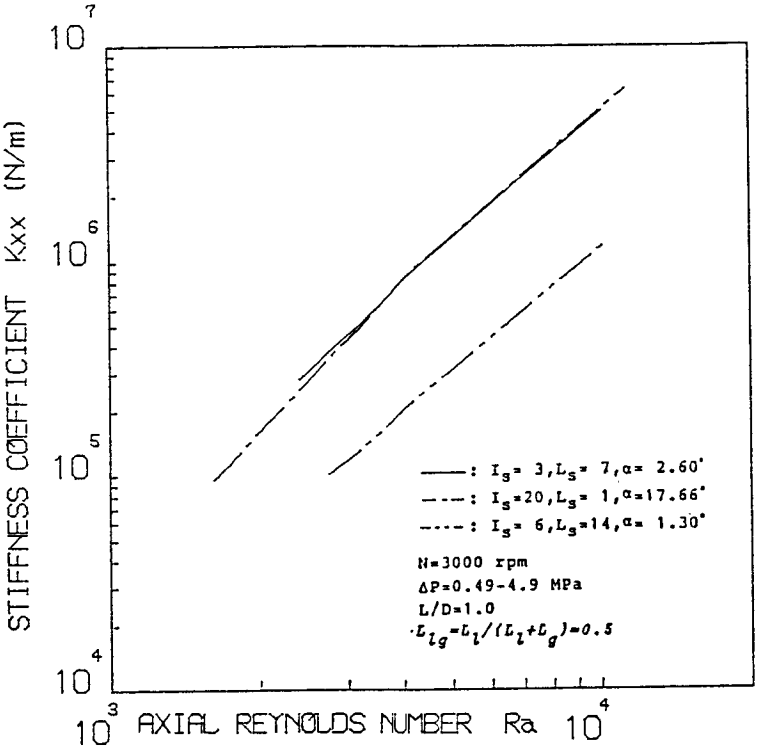

(a) Stiffness coefficient, K_{xx}.

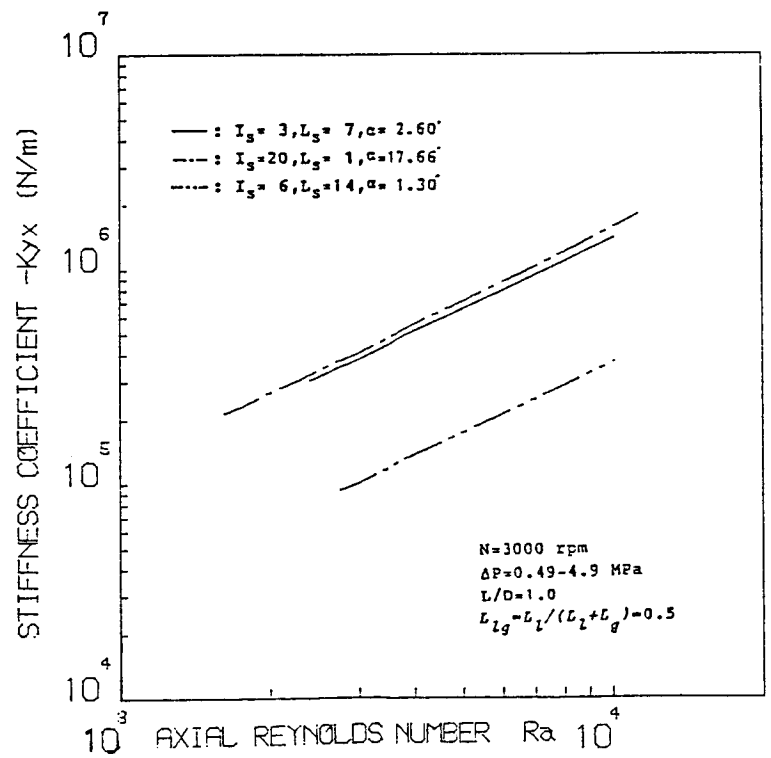

(b) Stiffness coefficient, K_{yx}.

Figure 6. - Effects of axial Reynolds number and spiral angle.

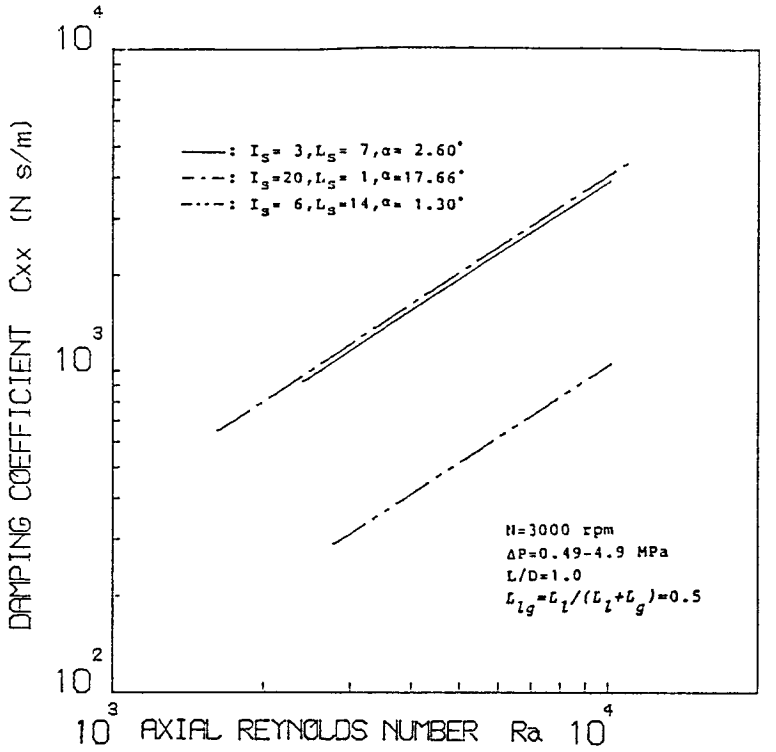

(c) Damping coefficient, C_{xx}.

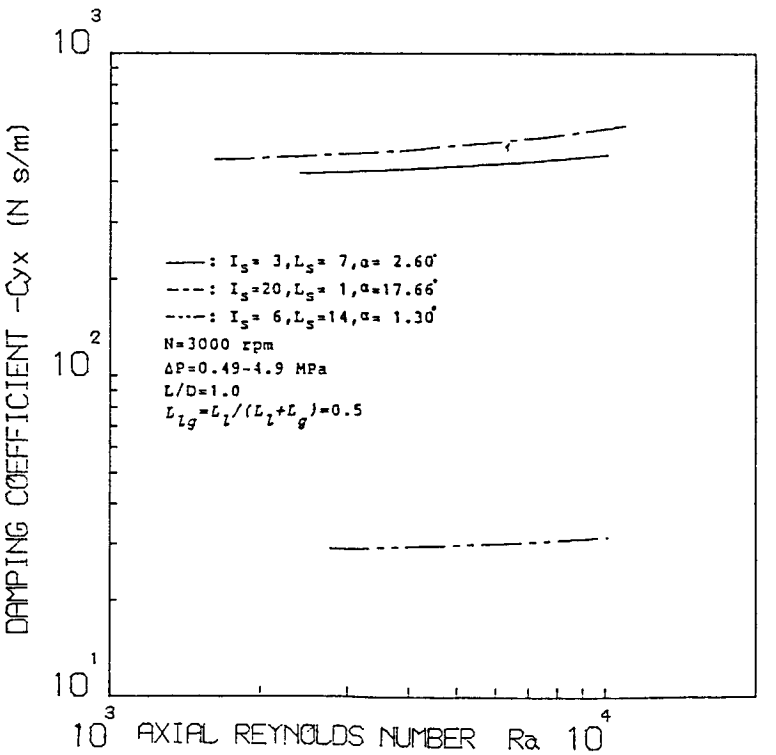

(d) Damping coefficient, C_{yx}.

Figure 6. - Continued.

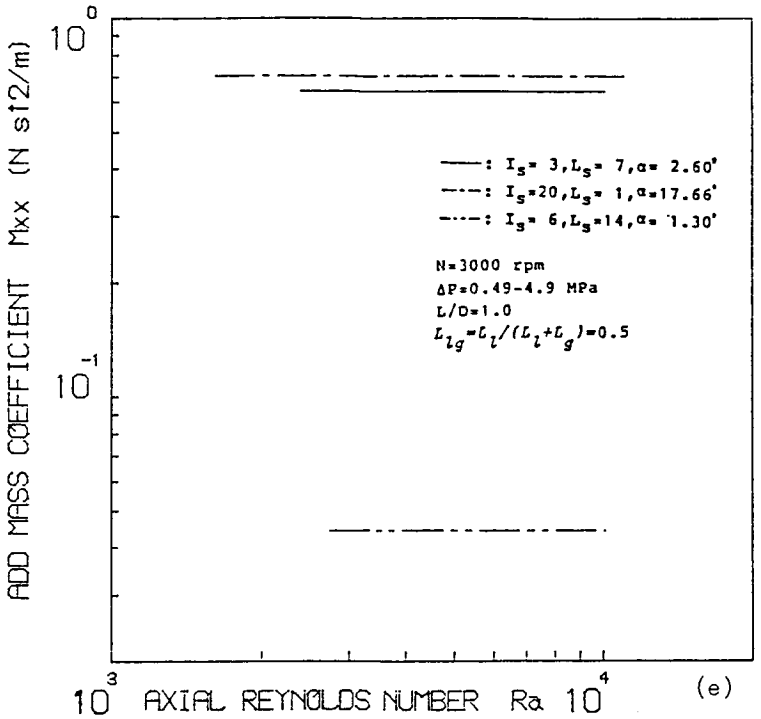

(e) Add mass coefficient, M_{xx}.

Figure 6. - Concluded.

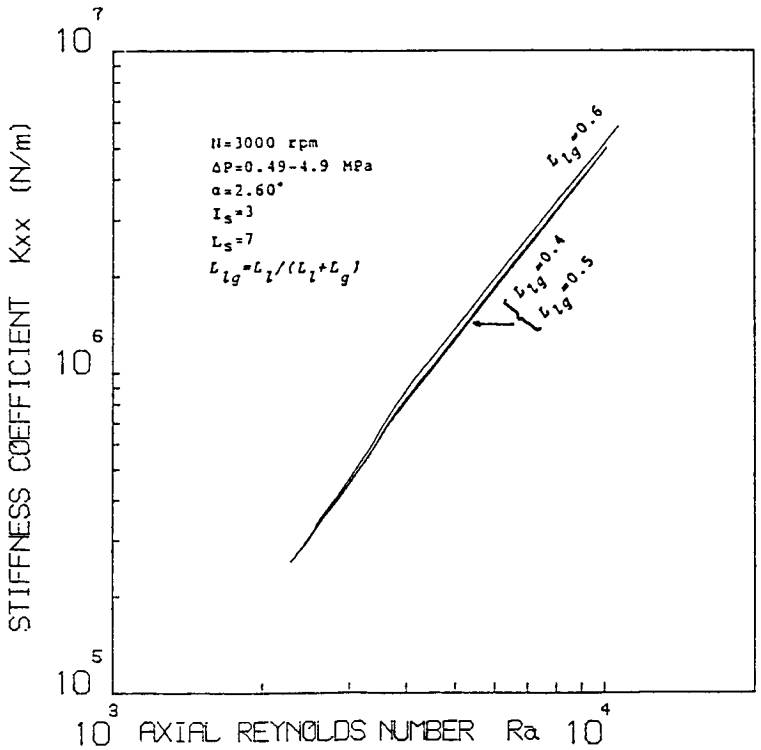

(a) Stiffness coefficient, K_{xx}.

Figure 7. - Effects of axial Reynolds number and ratio of land width to groove width.

C-3

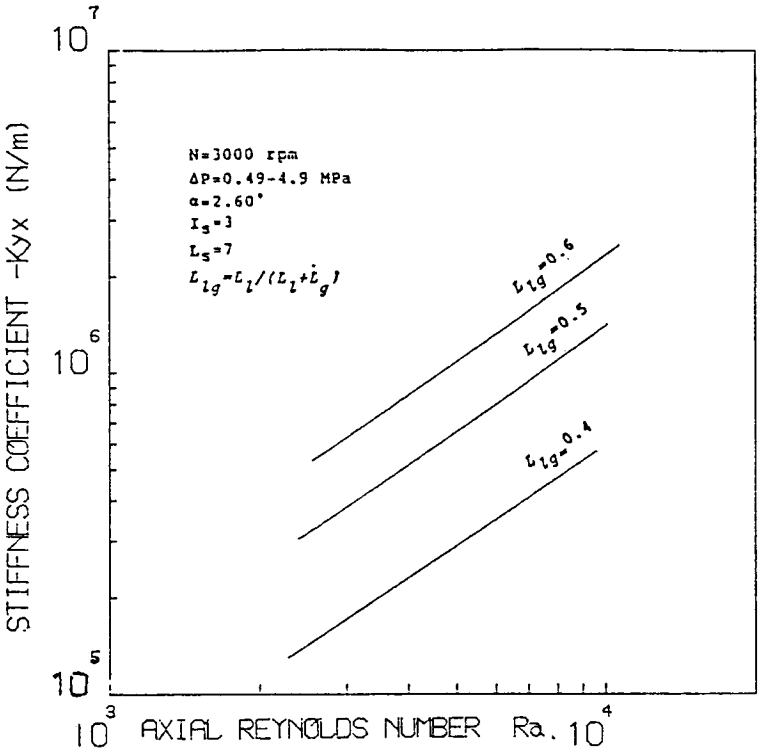

(b) Stiffness coefficient, K_{yx}.

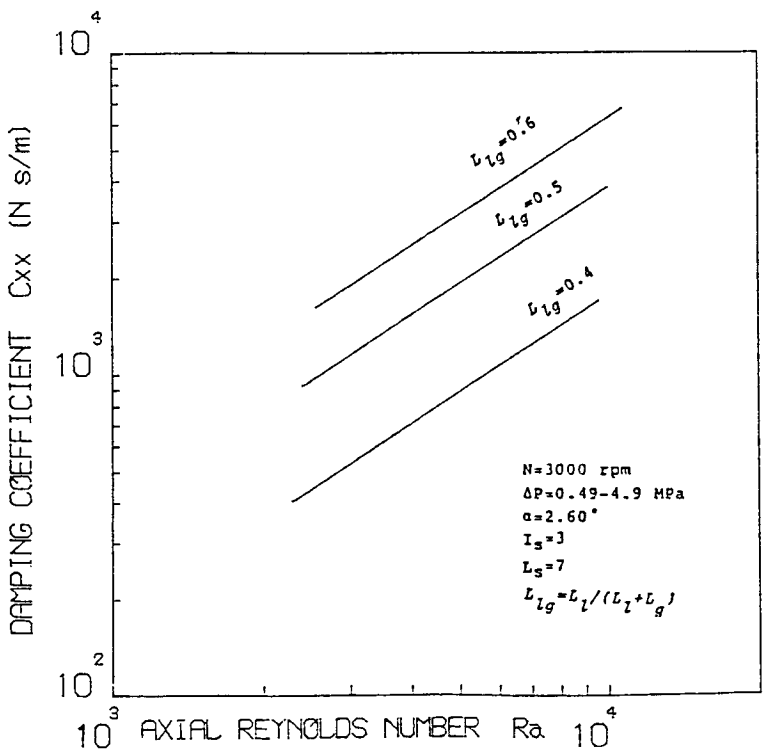

(c) Damping coefficient, C_{xx}.

Figure 7. - Continued.

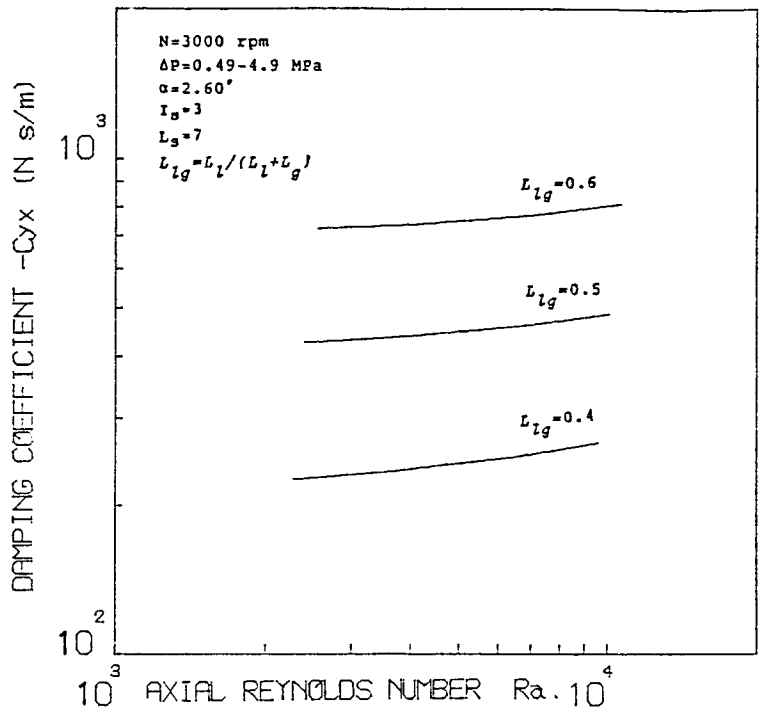

(d) Damping coefficient, C_{yx}.

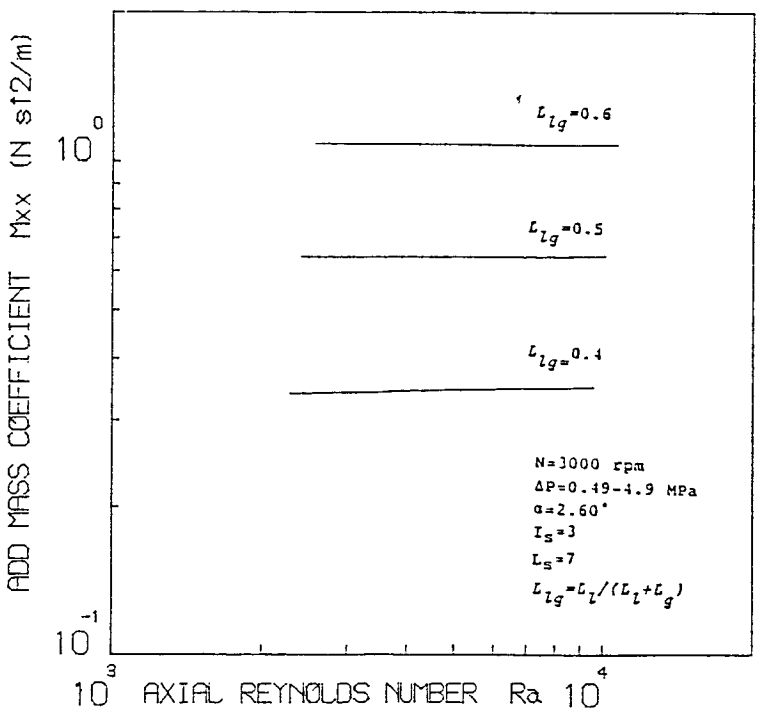

(e) Add mass coefficient, M_{xx}.

Figure 7. - Concluded.

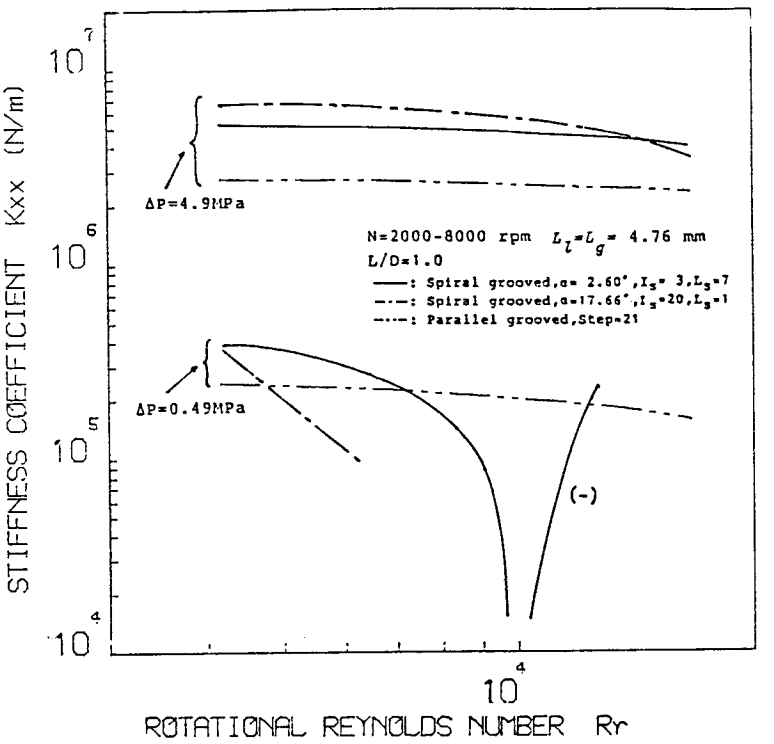

(a) Stiffness coefficient, K_{xx}.

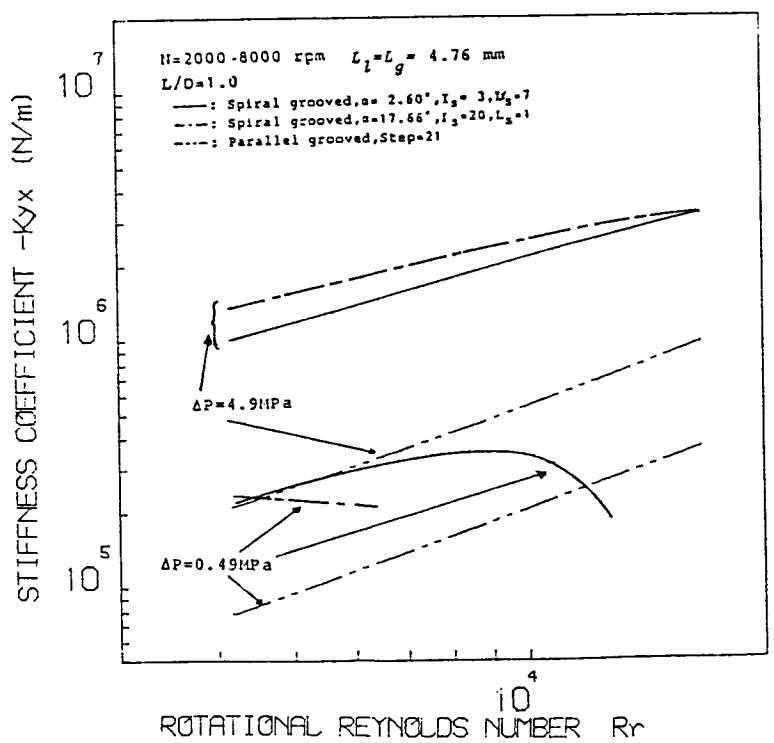

(b) Stiffness coefficient, K_{xx}.

Figure 8. - Effects of circumferential Reynolds number.

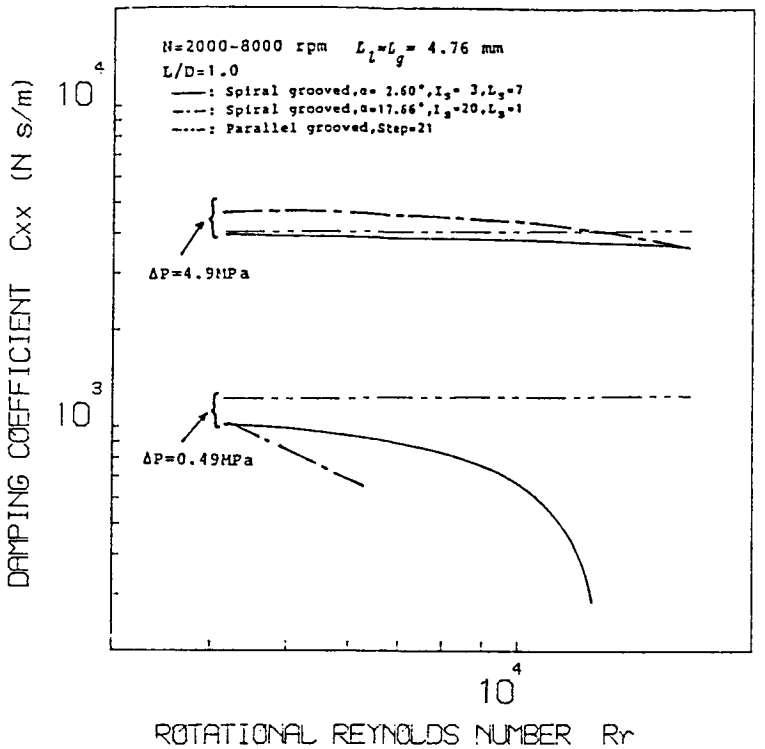

(c) Damping coefficient, C_{xx}.

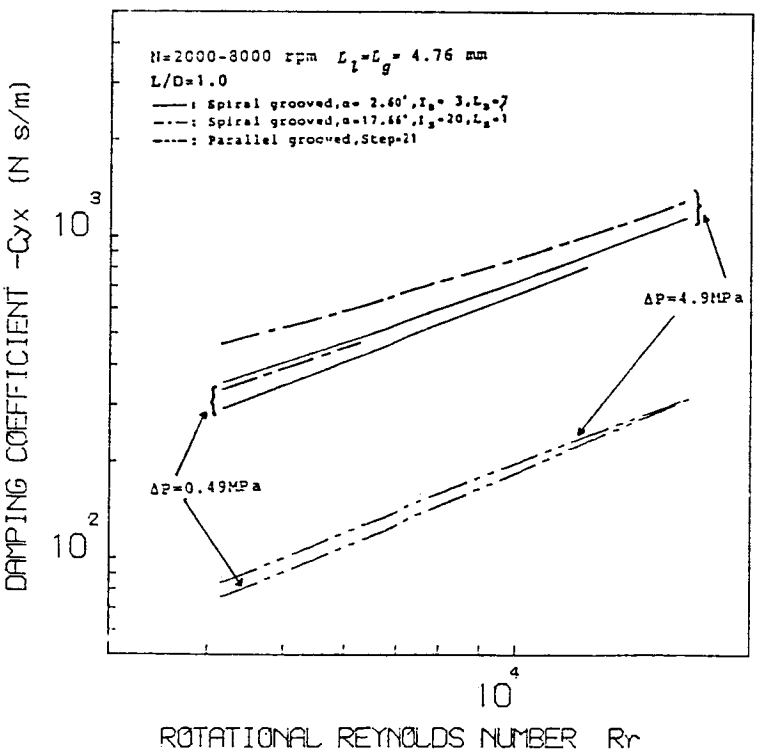

(d) Damping coefficient, C_{yx}.

Figure 8. - Continued.

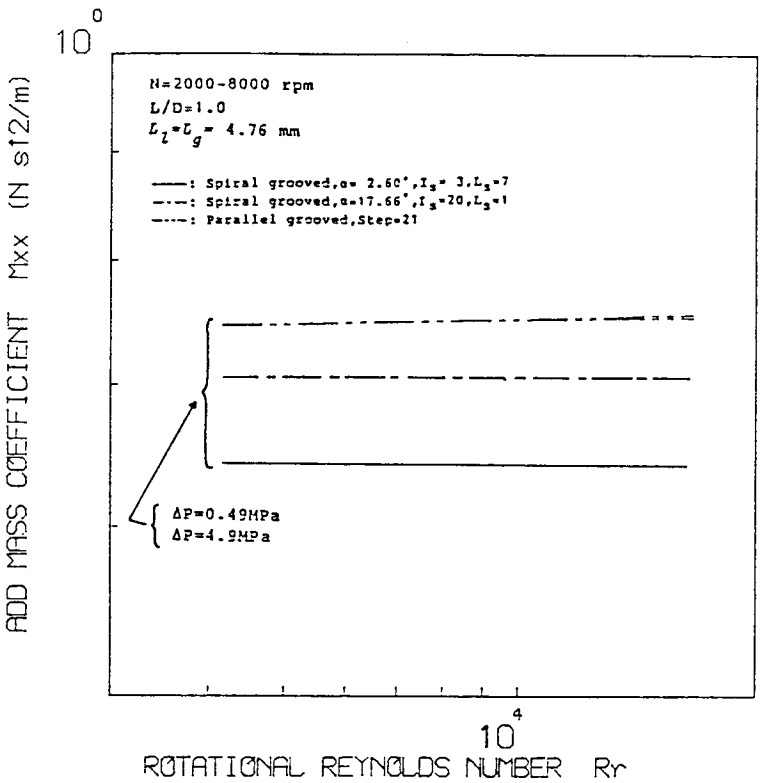

(e) Add mass coefficient, M_{xx}.

Figure 8. - Concluded.